A new approach to estimate pollutant emissions based on trajectory modelling and its application in the North China Plain

W. Y. Xu[1], C. S. Zhao[1], P. F. Liu[1], L. Ran[1], N. Ma[1], Z. Z. Deng[1], W. L. Lin[2], P. Yan[2], X. B. Xu[2]

[1]{Department of Atmospheric and Oceanic Sciences, School of Physics, Peking University, Beijing, China}

[2]{Key Laboratory for Atmospheric Chemistry, Centre for Atmosphere Watch and Services, Chinese Academy of Meteorological Sciences, China Meteorological Administration, Beijing, China}

Correspondence to: C. S. Zhao (zcs@pku.edu.cn)

Abstract

Emission information is crucial for air quality modelling and air quality management. In this study, a new approach based on the understanding of the relationship between emissions and measured pollutant concentrations has been proposed to estimate pollutant emissions and source contributions. The retrieval can be made with single point in-situ measurements combined with backward trajectory analyses. The method takes into consideration the effect of planetary boundary layer height on pollutant mixing and transport and accounts for wet deposition processes. It is independent of energy statistics, therefore can provide frequent updates on emission information. The spatial coverage can be further improved by using measurements from several sites and combining the derived emission fields. The method was applied to yield the source distributions of black carbon (BC) and CO in the North China Plain (NCP) using in-situ measurements from the HaChi (Haze in China) Campaign and to evaluate contributions from specific areas to local concentrations at the measurement site.

Results show that an emission field for the NCP that is comparable to the INTEX-B inventory can be retrieved and directly applied to quantify areal source contributions. Uncertainty analyses show that in-situ measurements of CO and BC bear errors below 0.1ppm and 12%, respectively. WRF model underestimates the PBLH under stable conditions. On average, an error of 1% in the modelled PBLH results in 1% variation in the derived emissions. The

uncertainty of the wet deposition ranges from 0 to 21% across the domain, while the trajectory displacement errors are mostly within 1.5 times of the grid size.

1 Introduction

Emission inventories are crucial for the modelling of gaseous and particulate pollutants and for the establishment of air quality management strategies, for which both local emissions and transport of pollutants need to be considered.

A fundamental problem of air quality modelling is that, it depends on the assumption that emission inventories are accurate. Chemical transport models are very sensitive to emission inventories. Different emission inventories may results in vastly different modelling outcomes (Ma et al., 2004). The most common approaches of deriving emissions can be divided into "bottom-up" and "top-down" methods. "Bottom-up" methods integrate the emissions from all known source types using energy statistics (e.g. statistical data on energy consumption by power plants, industries, various production sectors and residential combustion, etc.) and emissions factors (Wang et al., 2012; Zhao et al., 2012), which bear large uncertainties and cannot be easily updated (Zhang et al., 2009). Emissions may have large spatial and temporal variations, due to new policies and the rapid development, especially in developing countries such as China. "Top-down" retrieving techniques were initially based on the thought of spatially disaggregating the known total emission with the aid of statistical indicators (e.g. population, land-use, etc.). More recent developments in the "top-down" method resort to inverse modelling approaches, incorporating atmospheric observations (i.e. satellite observations or in-situ measurements) and chemistry transport models together with prior emissions as constraints to derive optimized emissions (Lin et al., 2007; Brioude et al., 2011; Lee et al., 2011). However, both satellite data and air quality models usually exhibit large uncertainties. Out-dated or inaccurate emission inventory poses a profound problem for air quality modelling and may result in wrong implications for future emission controls. Therefore, alternative approaches need to be developed, so that emission inventories can be updated or corrected.

Efforts in improving the temporal resolution were made by combining air quality measurements with trajectory analyses to yield source distributions. Early methods were mainly based on classification or clustering of trajectories (Miller, 1981; Moody and Samson, 1989; Harris and Kahl, 1990), which could only roughly identify sectors associated with high

pollution. Although such methods were not able to yield the spatial distribution of pollutant sources, they were still often used to distinguish different air masses and their accompanied pollutant concentrations (Lin et al., 2009; Tang et al., 2009) or to identify possible source regions on a larger scale (Liu et al., 2009). Ashbaugh (1983) and Ashbaugh et al. (1985) developed a statistical method, which was later on termed as the Potential Source Contribution Function (PSCF) analysis by Zeng and Hopke (1989). It is defined as:

$$PSCF(m,n) = \frac{t(m,n)}{T(m,n)}, \quad (1)$$

where *T(m,n)* is the total number of endpoints falling within the grid (m,n), and *t(m,n)* is the subset of endpoints that are on trajectories associated with concentrations above a certain criterion. In recent years, the PSCF analysis has been widely applied to identify possible pollutant source regions (Lucey et al., 2001; Ara Begum et al., 2005; Zhou et al., 2004). However, it can only yield a probability distribution of source regions and cannot quantify the source strength. Seibert et al. (Seibert et al., 1994) proposed the concentration field analysis (CFA) method, which calculates a logarithmic mean concentration for each grid on the domain of the trajectory analyses following the equation:

$$\overline{C}_{mn} = \frac{1}{\sum_{l=1}^{M} \tau_{mnl}} \sum_{l=1}^{M} \log(c_l)\tau_{mnl}, \quad (2)$$

where m and n are indices of the horizontal grid, l is the index of the trajectory, M the total number of trajectories, c_l the concentration at the receptor site at the time upon which trajectory l arrives and τ_{mnl} the residence time of trajectory l in grid (m,n). This method takes into account information from all the trajectories and in-situ measurements and made it easier to evaluate uncertainties of the outcome. Stohl et al. (1996) improved the method by using $\overline{C}_{mn}$ as a first guess, $10^{C_{mn}(i)/\overline{C}_{mnl}}$ ($i=1,\ldots,N_l$, N_l being the number of grids on trajectory l) as a weighting factor for each trajectory, and iterating the processes until the average difference between the concentration fields of two successive iterations is below 0.5% (Redistributed Concentration Field Analysis, RCFA). Such concentration field analyses are often used to detect possible plumes or yielding the regional distribution of pollutants (de Foy et al., 2007). RCFA solved the problem that the CFA attributes the receptor concentration c_l equally to all parts of trajectory l, however, iteration techniques often face the problem of convergence and "hot spots" on the first guess field are amplified while information of the

other sections on the same trajectories with the "hot spots" easily get lost through iterations. A common problem with these CFA techniques is that they yield logarithmic mean concentration fields and one cannot directly derive emission rates from those, or quantify the contributions of source regions to the receptor site. Seibert (2000, 2001) proposed an analytical inversion method for updating emissions, which has been improved by Eckhard et al. (2008) to allow for an a priori for the unknown sources and applied an iterative algorithm for ensuring solutions with only positive values. The method was further expanded by Stohl et al.'s (2009) work, in which they considered a baseline in the observations and provided a more detailed quantification of errors. The general theory is to retrieve *n2* unknowns in vector $\boldsymbol{x}$ (including gridded emission values and free parameters describing the baseline) from the equation $\boldsymbol{M(x-x^a)\approx y^o-Mx^a}$, where $\boldsymbol{x^a}$ is the a priori source vector, $\boldsymbol{y^o}$ contains *n1* observation values, matrix $\boldsymbol{M}$ of the size $n1\times n2$ contains the sensitivities of the atmospheric concentrations to the sources and is obtained from *n2* FLEXPART backward simulations (Seibert and Frank, 2004). A Bayesian inversion minimizing a corresponding cost function is performed to obtain the source vector $\boldsymbol{x}$. Such a method finally made it possible to update emission fields based on in-situ observations and trajectory-like output from the Lagrangian particle dispersion model, which is a huge development. However, calculations are very complex and are dependent on the a priori emissions to ensure that the inversion problem is not ill-conditioned due to insufficient information from the observations. Also, none of the above methods consider the influence of the boundary layer on pollutant concentrations, mixing and transport.

A new alternative method based on the understanding of the relationship between emissions and measured pollutant concentrations will be presented in this work, mainly focusing on the transport of pollutants within the planetary boundary layer (PBL). The application of the new method on deriving black carbon (BC) and CO emission fields and assessing source contributions will also be shown along with the uncertainties this method might bear.

2 Methodology

2.1 Site and measurements

Measurements of BC and CO were conducted at the Wuqing Meteorological Station, located at a suburban district between Beijing and Tianjin and surrounded by Hebei Province. This

site has proved to be highly representative of the overall pollution level of the polluted NCP region and a favourable spot for observing transport of air pollutants (Xu et al., 2011).

A Multi-angle Absorption Photometer (MAAP Model 5012, Thermo, Inc., Waltham, MA USA) was employed to measure BC mass concentration in unit of $\mu g \cdot m^{-3}$, while CO was measured with a gas filter correlation analyser (TE 48C, Thermo Environmental Instruments Inc., USA), and recorded as 1-min average mixing ratios by volume (ppbv). Meteorological variables were obtained by an Automatic Weather Station installed at the Wuqing Meteorological Station. Details on the measurement site, instruments, data maintenance and calibration are described by Ma et al. (2011) and Xu et al. (2011).

Time series of hourly average black carbon mass concentration, CO volume mixing ratio, wind speed and wind direction, WRF PBL height (PBLH) and accumulated hourly precipitation is shown in fig.1. During the campaign, 10 precipitation events were observed, mostly with precipitation durations of 1-4 hours, except for the rain event on 17th Jul., which lasted for 14 hours. After subtracting hours with no valid observations, 725 data points for BC and 782 data points for CO remain and are utilized in the emission retrieval.

2.2 WRF simulations

The ARW (Advanced Research WRF version 3.1.1) model is used to generate high resolution meteorology fields for the backward trajectory study with the Hybrid Single Particle Lagrangian Integrated Trajectory (HYSPLIT) model. An 18km/6km two-way nested grid was applied in the simulation, with the outer domain covering an area of 3000km×3000km large (fig.2a). The model physics options used are WRF Single Moment Class 3 (WSM3) for microphysics parameterization, Rapid Radiative Transfer Model (RRTM) scheme (Mlawer et al., 1997) for longwave radiation processes, Dudhia scheme for short wave radiation (Dudhia, 1989), 5-layer thermal diffusion for land surface processes (Dudhia, 1996), Yonsei University non-local scheme for boundary layer parameterization (Hong et al., 2006), Kain-Fritsch scheme (Kain and Fritsch, 1993) for cumulus parameterization. The simulation period is from 11 Jul. to 14 Aug., 2009. The period was split into several runs, with each run simulating 3 days and 12 hours. The model was initialized every 3 days at 12UTC and integrated over 84 hours. The first 12h of each run was discarded due to model spin-up. The initial and boundary conditions required for ARW model integrations were adopted from the National Centers of

Environmental Prediction (NCEP) FNL (Final) Operational Global Analysis data at 1.0 degree resolution, which were updated every 6h.

2.3 Backward trajectory calculations and cluster analyses

The HYSPLIT model (version 4) from NOAA Air Resources Laboratory (Draxler and Hess, 1997; Draxler and Hess, 1998; Draxler, 1999) was used for the backward trajectory analyses, applying only the ARW output of the inner domain, which has a spatial resolution of 6km×6km and a temporal resolution of 1h. The trajectory endpoint is set to 39.38N and 117.02E with a height of 2 m above the ground level. 48 hours backward trajectories were calculated at a 1h interval from 13 Jul. to 14 Aug. 2009.

The trajectories were clustered into 4 groups using the clustering tool of HYSPLIT 4 and the frequency distribution of trajectory height occurring with travel time is calculated.

2.4 Methodology of emission retrieval and areal source contribution assessment

2.4.1 General theory

Assuming that pollutant concentrations are well mixed within the PBL, emissions into a certain air mass can be estimated as the concentrations divided by the residence time. If we further presumed that all grids on the same trajectory *l* share the same pollutant concentrations, we would yield a uniform emission factor for all grids on *l*:

$$E_l = C_l / T_l , \quad (2)$$

where C_l stands for local vertical column mass concentrations upon arriving time of *l* at the receptor site, T_l is the residence time of *l* in the PBL. For CO, the measured values are given in volume mixing ratios (γ_{CO} , in *ppbv*). During daytime (9am-6pm), in the convective boundary layer (CBL), we assume that pollutant concentrations are well mixed and evenly distributed, thus $C_l(CO)$ can be calculated as:

$$C_l = \frac{\gamma_{CO} \cdot M_{CO} \cdot P}{R \cdot T} \cdot PBLH , \quad (3)$$

where M_{CO}, P, T, R and PBLH respectively stand for the molar mass of CO, atmospheric pressure, temperature, ideal gas constant and the planetary boundary layer height. From the late afternoon to the early morning, in the stable boundary layer (SBL), we assume that concentrations are exponentially decreasing with height, with the PBLH being the e-folding height, thus $C_l(CO)$ can be given by:

$$C_l = \frac{\gamma_{CO} \cdot M_{CO} \cdot P}{R \cdot T} \cdot \int_{z=0}^{\infty} e^{-\frac{z}{PBLH}} dz \,. \quad (4)$$

BC measurements are given as mass concentrations (m_{BC}, in $\mu g \cdot m^{-3}$), thus the column mass for the CBL and SBL conditions can be respectively calculated as:

$$C_l = m_{BC} \cdot PBLH \quad (5)$$

and

$$C_l = m_{BC} \cdot \int_{z=0}^{\infty} e^{-\frac{z}{PBLH}} dz \,. \quad (6)$$

Trajectories cross each other's paths, and each grid *(m,n)* will be associated with multiple emission values, by averaging them, we get the mean emission rate of *(m,n)*:

$$\overline{E}_{mn} = \overline{\sum_{l=1}^{M} C_l \cdot A_{mn} / T_l}^{mn}, \quad (7)$$

where M is the total number of trajectories and $A_{m,n}$ is the area of grid (m,n).

2.4.2 Weighting factor

Considering that it might be unrealistic to assume that all grids on *l* have the same emission rate, especially when *l* travels a long distance and crosses over major emission sources, the method can be improved by introducing a weighting factor *W*:

$$W_{mn} = \frac{F_{mn}}{\overline{F}_{mnl}}, \quad (8)$$

where *F* should be the field of a variable that is closely related to the emission of our target and can serve as a priori to the emission field analyses, e.g. population, NO_2 column distribution, aerosol optical depth (AOD) distribution or previous emission inventories. $\overline{F}_{mnl}$ is the average value of *F* for the grids *(m,n)* that *l* travels over. In this study, the average distribution of Moderate-resolution Imaging Spectroradiometer (MODIS) Aerosol Optical Depth (AOD, fig.2b) and Ozone Monitoring Instrument (OMI) tropospheric NO_2 column amount (fig.2c) in 2009 were applied as the weighting factor for BC and CO emissions. AOD can reflect to a certain extent the distribution of aerosol columnar loading and NO_2 is short-lived in the atmosphere, suggesting that its distribution is closely related to emissions. The average emission field weighted with a priori field can be acquired by:

$$\overline{E}_{mn} = \overline{\sum_{l=1}^{M} W_{mn} \cdot C_l \cdot A_{mn} / T_l}^{mn} \,. \quad (9)$$

2.4.3 Residence time calculation

The method used to determine the residence time of trajectory l is shown in fig.3a. The residence time is defined as the time the air parcel stays within the boundary layer. First, the PBLH values on the grids (m,n) by the time trajectory l passes through them are extracted from the WRF meteorology simulations. Then, we start at the time upon which l arrives at the receptor site (t_1) and go back in time, for each time step of l, it is to be determined whether the trajectory has reached above the according PBLH. This is proceeded until the first time step where l reaches the PBL height (t_h). The PBL residence time T_l is thus determined as:

$$T_l = t_1 - t_h . \tag{10}$$

2.4.4 Wet deposition

For water soluble atmospheric contents, correction for wet deposition is of certain necessity. Although CO is only weakly soluble in water and thus is unlikely to be largely influenced by precipitation events, we provide a method for wet deposition correction for gases to make our method applicable also for other gas pollutants.

According to the Henry's law, for gas a:

$$[a(aq)] = H_a \cdot P_a = H_a \cdot \gamma_a \cdot P , \tag{11}$$

where $[a(aq)]$ is the aqueous phase concentration of a (mol·L^{-1}) in raindrops, H_a is the Henry's law coefficient for a (H_{CO}=1600 M·atm^{-1}, Sander, 1999) and P_a is the partial pressure of a in the atmosphere (atm).

Assuming that all of *a(aq)* fell together with the raindrops to the ground, then the total amount of scavenged a (in g·m^{-2}) can be estimated as:

$$C_{a,wet} = [a(aq)] \cdot 10^3 \cdot M_a \cdot P_r \cdot 10^{-3} = H_a \cdot \gamma_a \cdot P \cdot M_a \cdot P_r , \tag{12}$$

where M_a is the molar mass of gas a, P_r (mm) is the hourly average precipitation amount over a unit area (1 m^2). To avoid using the mixing ratio that is probably already influenced by precipitation, we calculate the wet deposition amount with the γ_a that was observed an hour ahead of each precipitation record.

First, the local column concentration (C_a) that is used in eq. 9 should be corrected for wet deposition.

$$C_a^{'} = C_a + C_{a,wet} = \begin{cases} (1 + H_a \cdot P_r \cdot R \cdot T / PBLH) \cdot C_a , & 9a.m. \le hr \le 6p.m \\ (1 + H_a \cdot P_r \cdot R \cdot T \Big/ \int_{z=0}^{\infty} e^{-\frac{z}{PBLH}} dz) \cdot C_a , & hr < 9a.m. \, or \, hr > 6p.m \end{cases} \quad (10)$$

By defining a wet scavenging correction coefficient in the form of:

$$k_{wet}^{a} = \begin{cases} (1 + H_a \cdot P_r \cdot R \cdot T / PBLH) , & 9a.m. \le hr \le 6p.m \\ (1 + H_a \cdot P_r \cdot R \cdot T \Big/ \int_{z=0}^{\infty} e^{-\frac{z}{PBLH}} dz), & hr < 9a.m. \, or \, hr > 6p.m \end{cases} , \quad (13)$$

the corrected column mass concentration can be obtained by:

$$C_a^{'} = k_{wet}^{a} \cdot C_a . \quad (15)$$

Column concentrations along the track also need to be corrected with the wet scavenging correction coefficient for all grids *(m,n)* that trajectory *l* travels through:

$$\overline{E}_{mn} = \overline{\sum_{l=1}^{M} W_{mn} \cdot k_{wet,mn}^{a} \cdot C_{a,l}^{'} \cdot A_{mn} / T_l}^{mn} = \overline{\sum_{l=1}^{M} W_{mn} \cdot k_{wet}^{a} \cdot k_{wet,mn}^{a} \cdot C_{a,l} \cdot A_{mn} / T_l}^{mn} , \quad (16)$$

where $k_{wet}^{a} = \begin{cases} (1 + H_a \cdot P_{r,mn} \cdot R \cdot T_{mn} / PBLH_{mn}) , & 9a.m. \le hr \le 6p.m \\ (1 + H_a \cdot P_{r,mn} \cdot R \cdot T_{mn} \Big/ \int_{z=0}^{\infty} e^{-\frac{z}{PBLH_{mn}}} dz), & hr < 9a.m. \, or \, h > 6p.m \end{cases}$. (17)

Black Carbon aerosols (BC) are mostly submicron particles with sizes of 0.3-0.4μm (Yu et al., 2010; Hitzenberger and Tohno, 2001), which are part of the accumulation mode (0.05-2μm). Ultrafine particles (<0.05μm) easily come into contact with raindrops through Brownian diffusion, while larger particles (2-20μm) are easily caught by raindrops through impaction and interception (Slinn et al., 1978). Those two effects are weak for the accumulation mode particles, which mainly depend on acting as CCN (cloud condensation nuclei) and developing into cloud drops to get scavenged from the atmosphere. However, BC aerosols are hydrophobic particles that are not soluble in water, thus are mostly CCN-inactive (Kuwata and Kondo, 2008). Aged BC aerosols are often coated with water soluble substances, which make them more hydrophilic. Wet scavenging coefficients (k_s) for water soluble particles are often parameterized in the form of:

$$k_s = a \cdot Pr^{b} \quad (18),$$

with *a* in the range of 0.36 to 1.28 and *b* in the range of 0.64 to 0.78 (Constantin, 2004). If we

want to apply a similar parameterization for BC, we have to know the fraction of core-shell mixed BC that can be wet deposited (f_{wet}).

North China Plain is abundant in highly hygroscopic particles (Liu et al., 2011), thus thinly coated BC particles have rather small chances in becoming activated or washed out. Shiraiwa et al. (2007) investigated the evolution of the BC mixing state in Tokyo and found out that during polluted days, the number fraction of thickly coated BC particles ranged from 0.07 to 0.42, revealing a clear diurnal cycle that is lower during the night and higher during the day. According to their work, we make the assumption for the diurnal variation of f_{wet} as is shown in fig.3b.

The wet scavenging of BC is parameterized as:

$$C_{BC,wet} = f_{wet} \cdot k_s^{BC} \cdot C_{BC} = f_{wet} \cdot a \cdot Pr^b \cdot C_{BC} \tag{19}$$

Similar to the wet deposition correction for gases, the correction for BC can be given as:

$$C'_{BC} = C_{BC} + C_{BC,wet} = (1 + f_{wet} \cdot a \cdot Pr^b) \cdot C_{BC} = k_{wet}^{BC} \cdot C_{BC} \ , \tag{20}$$

$$\overline{E}_{mn} = \overline{\sum_{l=1}^{M} W_{mn} \cdot k_{wet,mn}^{BC} \cdot C'_{BC,l} \cdot A_{mn} / T_l}^{mn} = \overline{\sum_{l=1}^{M} W_{mn} \cdot k_{wet}^{BC} \cdot k_{wet,mn}^{BC} \cdot C_{BC,l} \cdot A_{mn} / T_l}^{mn} , \tag{21}$$

with k_{wet}^{BC} being the wet scavenging correction coefficient for BC at the receptor point and $k_{wet,mn}^{BC}$ the correction coefficient for the grids trajectory *l* passes through. The parameters *a* and *b* in eq. (13)-(14) are set as 0.8 and 0.7, respectively.

2.4.5 Contribution calculation

With the calculated mean emission field, the pollutant contributions of specific source regions to the receptor site can be easily assessed. The receptor site concentration contribution of each grid (in *g*) can be calculated as:

$$\overline{CB}_{mn} = \overline{E}_{mn} \cdot \tau_{mn} \ , \tag{22}$$

where τ_{mn} is the total residence time of all trajectories within the PBL in grid *(m,n)*.

$\overline{CB}_{mn}$ for CO can be converted into volume mixing ratio by:

$$\overline{CB}'_{CO,mn} = \frac{\overline{CB}_{CO,mn} \cdot R \cdot \overline{T}_{mn}}{A_{mn} \cdot M_{CO} \cdot \overline{P}_{mn} \cdot \overline{PBLH}_{mn}} \ , \tag{23}$$

while $\overline{CB}_{mn}$ for BC as mass concentrations can be obtained by:

$$\overline{CB}'_{BC,mn} = \frac{\overline{CB}_{BC,mn}}{A_{mn} \cdot \overline{PBLH}}$$

where $\overline{T}_{mn}$, $\overline{P}_{mn}$, $\overline{PBLH}_{mn}$ respectively stand for the average temperature, pressure and PBLH on grid (m,n).

In this study, the concentration contributions of local emissions in Wuqing and the transport contributions of Beijing, Tianjin and Hebei Province were assessed. Instead of τ_{mn}, the average daily residence time (total residence time divided by the days of the trajectory analyses (32 days)) was applied to acquire an average daily concentration contribution. For each source region evaluated, the spatial mean, minimum and maximum daily concentration contributions $\overline{CB}'_{mean}$, $\overline{CB}'_{\min}$ and $\overline{CB}'_{\max}$ were acquired by averaging $\overline{CB}'_{mn}$ over the grids or taking the minimum and maximum grid value within the bounds of the region. Accordingly, mean concentration contribution fractions could be calculated by:

$$\bar{f}_i = \frac{\overline{CB}_i}{\sum_i \overline{CB}_i} \times 100\%, i = 1,...,8, \quad (23)$$

where i stands for the different regions assessed in this study.

This method of emission retrieval is straightforward and can be accomplished based on single site measurements. Traditional bottom-up emission estimates depend highly on energy statistics, which take a long time to be updated and are crucial to the accuracy of emission inventories (Akimoto et al., 2006). Our retrievals can be frequently updated benefitting from the high temporal resolutions of ground measurements. The method is widely applicable for pollutants with longer lifetimes than the time used to constrain trajectories. It can be used for analyses of seasonal variations in emissions or areal contributions, if provided long-term monitoring data. It should be noted that by only taking into account trajectories within the PBL, the emission field is restricted to a limited distance range. However, improvements can be made by using measurements from several sites, which would compensate for the lack in spatial coverage.

2.5 Methodology of uncertainty analysis

2.5.1 Uncertainty introduced by PBLH modelling errors

The PBLH assumptions in our method have three kinds of influences on derived emissions. First of all, since the PBLH determines the residence time, an underestimation of PBLH would reduce the coverage of the derived emission field or the sample numbers in certain grids, because once the trajectory height exceeds the PBLH, it will not be taken into account anymore. Secondly, an underestimation in PBLH would give shorter residence time, which results in higher emission estimates according to eq.7. PBLH is also used to calculate C_l, an underestimation in PBLH would result in the underestimation of C_l and lower emission estimates. The latter two effects are coupled together.

To evaluate how the PBLH values influence the derived emissions, we introduced increments/decrements ($\delta PBLH$) of ±5%, ±10%, ±15%, ±25% into the modelled PBLH values.

A relative variation in the resulting emissions is calculated as:

$$\delta\overline{E}_{mn}^{PBLH} = \frac{\overline{E}_{mn}\left[(1+\delta PBLH)\cdot PBLH\right] - \overline{E}_{mn}\left[PBLH\right]}{\overline{E}_{mn}\left[PBLH\right]}, \tag{24}$$

where $\overline{E}_{mn}\left[PBLH\right]$ and $\overline{E}_{mn}\left[(1+\delta PBLH)\cdot PBLH\right]$ respectively represent the emissions derived with the modelled PBLH and that derived by the modelled PBLH added by a increment/decrement.

The influence of PBLH on the spatial coverage is evaluated by counting the grid number variation in respect to the standard case.

$$\delta N_{mn}^{PBLH} = \frac{N(\overline{E}_{mn}\left[(1+\delta PBLH)\cdot PBLH\right]) - N(\overline{E}_{mn}\left[PBLH\right])}{N(\overline{E}_{mn}\left[PBLH\right])}, \tag{25}$$

where N stands for the count of grids.

2.5.2 Uncertainty introduced by wet deposition parameters

Due to the complexity of atmospheric wet deposition processes, only parameterization schemes can be utilized to describe this process. Since for CO, wet deposition has minor influences ($<10^{-4}$%), the uncertainties won't be considered.

For BC, a wide range for the parameters in the wet deposition scheme has been reported, as already mentioned in Sect. 2.4.4. In the retrieval, we applied a mean value for *a* and *b* in eq. 18. The overall influence ratio of wet deposition on emissions can be calculated as:

$$\delta\overline{E}_{mn} = \frac{\overline{E}_{mn}(a=0.8,b=0.7) - \overline{E}_{mn}(a=0,b=0)}{\overline{E}_{mn}(a=0.8,b=0.7)}, \quad (26)$$

where $\overline{E}_{mn}(a=0.8,b=0.7)$ is the emission field of the standard retrieval and $\overline{E}_{mn}(a=0,b=0)$ the emissions retrieved not accounting for wet deposition. To explore how the possible range of wet deposition and influences on derived emissions, a relative error is calculated as:

$$\delta\overline{E}_{mn}^{wet} = \frac{\overline{E}_{mn}(a=1.28,b=0.78) - \overline{E}_{mn}(a=0.36,b=0.64)}{\overline{E}_{mn}(a=0.8,b=0.7)}, \quad (27)$$

where $\overline{E}_{mn}(a=1.28,b=0.78)$ and $\overline{E}_{mn}(a=0.36,b=0.64)$ respectively represent emission fields retrieved with maximum and minimum wet deposition.

3 Results and discussion

3.1 Trajectory frequency analyses

Figure 4(a1-a4) shows the 4 groups of trajectory clusters, while fig.4(a2-a4) displays the frequency distribution of various trajectory heights with their travel time. During the measurement period, the cluster groups in a1-a3 show similar occurrence frequencies, varying from 31.3%-38.9%, while the group from the north-eastern direction shows the lowest occurrence frequency (5.4%). Trajectories from the eastern (E) sector (group b: 38.9 %) reveal a circular flow that dominantly travels on lower altitudes and have longer residence times. They originate from Shandong Province, eastern Hebei or are maritime flows from the Bohai Sea, which travel over the industrial area and the inner city of Tianjin. The group from the southern (S) direction (group b: 34.1%) travels mostly from the southern inland to our receptor site and flows also stay on a relatively lower altitude before 30 hours of travel time, afterwards, flows tend to gain height. Group c has an occurrence frequency of 31.3%, including short circular flows from all directions and long straight flows from the north-western direction. The mean flow path is also circular and comes from the NW, traveling

altitude increases rapidly with time, indicating short residence times within the boundary layer. The cluster from the north-eastern direction mainly grouped trajectories together that rapidly descend to ground level 6-10 hours before arriving at the receptor point. Over 90% of those trajectories occurred during 23rd -25th July, in which period Wuqing experienced several precipitation episodes.

3.2 BC and CO emissions in the NCP

The emissions of BC and CO in China were assessed by Streets et al. (2001) for the year 1995 and by Zhang et al. (2009) for the year 2006. BC and CO exhibit important influences on the climate and human health (Cooke and Wilson, 1996; Ackerman et al., 2000), they both show increased emissions in 2006 compared to inventories in 1995. Many uncertainties still exist in the inventories, which need to be improved. BC aerosol and CO are both mainly released anthropogenically from fossil fuel combustion and biomass burning and naturally from forest fires (Jacobson, 2001). BC has a lifetime of one (±1) week (Ramanathan and Carmichael, 2008), while CO has a lifetime of 30-90 days on the global scale of the troposphere (Seinfeld and Pandis, 2006).

Figure 5(a2-a4) shows the retrieval results of average BC emission, using either no variable (a2), AOD distribution (a3) or NO_2 column amount (a4) distribution as weighting factor. Overall, the use of weighting factors shows no obvious influence on the distribution of emissions, indicating that the method can derive emission fields even without any a priori input.

Since trajectories are only used to the point where they reach out of the boundary layer, only the emission information of a limited region could be obtained. Average BC emissions are high in the northern part of Tianjin and Beijing Municipality and in north-eastern Hebei (Hebei-NE). Compared with the INTEX-B emission distribution, the retrieved distribution in the northern part is more even, while the emission distribution in southern Hebei (Hebei-S) and Shandong (south of Hebei) are more similar to the previous inventory. In respect to the INTEX-B 2006 emissions, Hebei-Langfang, which is situated between Beijing and Tianjin, shows the highest mean emission increase ($3.5 \cdot 10^{10}$ $\mu g \cdot hr^{-1}$, Tab.1), while mean emissions in Beijing barely changed. Tianjin and the Hebei-NE also show largely increased emissions.

Figure 5(b2-b4) show the calculated average CO emission field. From the distribution of emissions, it can be noted that the high centre of average emissions in Hebei-NE and Hebei-

Langfang are more pronounced than those estimated by the INTEX-B inventory, while in the urban centre of Tianjin, emissions are not that obvious in comparison. Average CO emissions are most prominent in Hebei-NE, with a spatial mean and maximum of $25.5 \cdot 10^{12}$ and $41.4 \cdot 10^{12}$ $\mu g \cdot hr^{-1}$(tab.1), respectively. Hebei-Langfang and Tianjin also revealed very high emission values, with mean values reaching $21.2 \cdot 10^{12}$ and $21.1 \cdot 10^{12}$ $\mu g \cdot hr^{-1}$, respectively. Compared to the emissions in 2006, CO emissions have significantly increased by 2-5 times.

Since trajectories cross each other's path, multiple values are assigned to each grid and are averaged to obtain the final emissions. Standard deviations have been calculated for all grids, and the spatial mean, minimum and maximum standard deviations of emissions for 6 sectors including Tianjin, Beijing, Hebei NE, Hebei-Langfang and southern Hebei within and out of 100km distance (Hebei-S($d<100$km), Hebei-S($d \geqslant 100$km)) are listed in tab.2. Standard deviations are comparable to the derived emissions for both BC and CO. The standard deviations are 0.5-1.0 times the values of the derived mean emissions. Both the temporal variation of emissions and the modelling errors (including uncertainties in measurements, PBLH modelling, wet deposition parameterization and trajectory position errors, etc.) contribute to the standard deviations. Since our method is based on statistical analysis, the retrieval only provides the total emission on each grid. It does not directly provide the locations of important sources and cannot differentiate between the emissions from the different source types. However, as is shown in Zhang et al.(2009), the share of emissions by each sector (transportation, residential, industry and power) has changed little during 2000-2006. Thus, a rough estimate could be made on the emission from different source sectors using their share of emissions as provided by the INTEX-B or other inventories.

Altogether, for atmospheric pollutants that have lifetimes longer than the time used to constrain trajectories, the emissions can be derived with the new approach. The spatial resolution of the retrieval might be improved either by applying higher spatial resolution mesoscale modelling or by replacing the simple backward trajectory model with more complicated trajectory models including dispersion processes. The spatial coverage and the accuracy of the retrieval can be increased by using data from a network of stations. This method can be widely applied to ground measurements all around the world and can be used in various senses. Emission inventories require extensive time and effort for wide range data collection, which often cannot keep up with the rapid changes in emissions of developing countries. This method provides a simple way to derive emissions that are up to date. It could

also be used to analyse seasonal variations in emissions using long-term pollutant monitoring results. However, knowing only the distribution of emissions is not enough for the establishment of pollution control strategies. The concentration contribution of source regions to local pollution levels is even more crucial and will be discussed in the next section.

3.3 Areal source contribution assessment

High emission centres might not exert great influences on local pollution levels, if air masses hardly travel over them, whereas other locations with comparatively insignificant emissions may have unnegligible influences, because they are often on the travel path. Hence it is the meteorology, upon which the concentration contributions of various emission source regions depend.

Table 3 summarizes the source contributions of Beijing, Tianjin and Hebei to local BC and CO concentrations in Wuqing and corresponding contribution fractions. BC emissions in Tianjin contribute 35-77 % to local concentrations, with spatial mean and maximum daily concentration contributions being 2.5 and 21.0 $\mu g \cdot m^{-3}$, making it the most dominant source contributor. The BC emissions in Hebei-S (d<100 km) also exert considerable influence on local BC concentrations, contributing on average 18.8 %. Maximum concentration contributions can reach up to 3.2 $\mu g \cdot m^{-3}$. Although Hebei-Langfang and Hebei-NE also showed high emission values, their mean contribution to BC concentrations in Wuqing are relatively lower (6.5 and 9.0 %).

For CO, similar results could be found. Emissions in Tianjin contribute 43.9-77.2 % to local concentrations, with mean daily concentration contributions being 507.0 ppb. Locations in Hebei S(d<100km) contribute 38.2-577.5 ppb to local CO concentrations, taking up 148.5% of the total on average. Hebei-Langfang and Hebei-S contribute on average 82.6 (8.9 %) and 77.2 ppb (8.3 %), which are also considerable amounts. Although the mean contribution of Beijing is moderate, its spatial maximum contribution can reach up to 206.0 ppb.

In all, areal source contribution assessments could be simply made based on the derived emissions and the residence time of trajectories. Results are in accordance with the conclusions from previous work (Xu et al., 2011).

3.4 Uncertainties of derived emissions

3.4.1 Uncertainties of the local measurements

The CO measurements were conducted using the 48C-series gas filter correlation analyser from Thermo Environmental Instruments. The instrument has a lower detection limit of 0.04 ppm, a zero noise of 0.02 ppm and a precision of ±0.1 ppm (Lin et al., 2009). The zero drift for 24hours is below 0.1 ppm, automatic zero checks were conducted every 6 hours. The linearity of the multipoint calibrations showed R^2 in the range of 0.9993 and 0.9998, with a 3% variation in linear slope.

BC mass concentrations were calculated using the measured absorption coefficients (σ_{ap}) from the MAAP instrument according to $\sigma_{ap}=m_{BC}\cdot 6.6 m^2/g$, where $6.6 m^2/g$ is the mass absorption efficiency (Ma et al., 2011). The uncertainty in σ_{ap} measured by MAAP was estimated to be below 12 % (Petzold and Schönlinner, 2004; Petzold et al., 2005).

3.4.2 Uncertainty of the boundary layer height

Recent researches have been focusing on the qualitative and overall assessment of the performance of various PBL schemes. The Yonsei University scheme that we used in this work has been proven to be the best performing PBL physics parameterization scheme, especially during summer (Hu et al., 2010; García-Díez et al., 2011). However, it was also reported that while many PBL schemes (including the YSU scheme) do well in unstable and weakly stable boundary layers, they give poor performance in stable boundary layers (Wu et al., 2011), with the YSU scheme only doing slightly better than other evaluated schemes.

As already introduced in Sect. 2.5.2, the modelled PBLH in our method have three kinds of influences on derived emissions. To determine how its effect on C_l and residence time influences the derived emissions, we introduced increments/decrements ($\delta PBLH$) of ±5%, ±10%, ±15%, ±25% into the modelled PBLH values and observed how derived emissions varied accordingly. As displayed in fig. 6a, the spatial coverage of emissions changes -8% to 13% with the induced PBLH decrements(increments). The relative emission field variations with $\delta PBLH$ ($\overline{\delta E}_{mn}^{PBLH}$) shows median values distributed along the 1:1 line (fig.6b), indicating that on average, 1% overestimate (underestimate) of the PBLH would accordingly result in a 1% overestimate (underestimate) of emissions. This results suggests that for most grids, the influence of PBLH on C_l dominates in the resulting errors, since C_l is proportional to PBLH

and varies almost linearly with it. The 25th-75th percentile of the $\delta\overline{E}_{mn}^{PBLH}$ are within a narrow range, whereas the 5th-95th percentile are widely distributed, which reveals that a part of the grids, especially those far from the receptor location, are affect by the reduction in residence time and sample number. Underestimating PBLH results in a smaller range of errors than that resulted from overestimating PBLH. For an underestimation of 25% the 5th to 95th percentile relative emission errors for BC and CO respectively range from -33% to -2% and from -34% to -6%.

3.4.3 Uncertainty of the BC wet deposition

Influence ratios of the BC wet deposition process and relative errors are calculated using the method described in Sect. 3.4.3. Overall, considering the wet deposition process for BC would yield an emission field that is on average 1.4% higher. A maximum influence ratio of 17.9% was observed under the standard settings of the wet deposition parameterization, indicating that the wet deposition impact on BC is not negligible. The total range of the parameters *a* and *b* in eq. 18 introduces an average relative error of 1.24% and a maximum error of 21.1% into the emission estimates. Although the maximum error seems to be high, the errors for 75% of the grids are below 1.3% and for 95% of the grids, errors fall within 4.7%, assuming that the range of the parameters provided in literature can cover the actual range wet deposition amount.

3.4.4 Uncertainty of the trajectory calculation

The accuracy of trajectories was mainly evaluated by tracer studies. Possible tracers are balloons, material tracers (e.g. smoke plumes or released inert tracer gases) or dynamical tracers (e.g. potential temperature or isentropic potential vorticity).

Baumann and Stohl (1997) evaluated trajectories against balloons. For a travel time of 46 hours, errors were below 20%. Assessments with material tracers suggest that for travel times within 60 hours, errors were around 10% (McQueen and Draxler, 1994). Stohl and Seibert (1998) used dynamical tracers and came to errors below 20% for a travel time of 120 hours. Stohl (1998) reported that the accuracy of trajectories has been improved since three dimensional wind fields were made available by numerical weather prediction models. They summarized the computation accuracy of trajectories and came to the conclusion that a position error of 20% of the travel distance is typical for calculated trajectories.

In our study, 48 hours backward trajectories were calculated using high resolution meteorology wind fields from the WRF model, which should be able to increase the accuracy of the trajectories. If we assume that position errors were 20%, we would get a maximum position error of 112km. Fig. 7a displays the occurrence of different travel time and position errors in the trajectory modelling results. Travel time for most trajectories is within 24 hours, while the occurrence of displacement errors shows a peak at 15 km, which is within one grid size. As can be noted from fig.7b, 75% of the trajectories travel less than 18 hours within the boundary layer and show displacement errors below 30km, which is roughly 1.5 times the grid size of our the retrieval.

4 Conclusions

In this study, a new method for air pollutant emission retrieval has been proposed and applied to estimating the source distributions and areal source contributions of BC and CO in the North China Plain.

The retrieval is accomplished based on single point in-situ measurements combined with high resolution mesoscale modelling and backward trajectory analyses. The impact of boundary layer height on pollutant mixing and transport and wet deposition processes are accounted for in the retrieval. The method can easily retrieve emissions in comparison to bottom-up and inverse modelling approaches. With long-term pollutant concentration monitoring data, seasonal and inter-annual variations in emissions can be analysed. In comparison with potential source contribution function and concentration field analyses techniques, which can only provide possible source locations/possible concentration distributions, our method can yield emission distributions, which can be directly compared to other inventories. It can also be directly used to evaluate areal source contributions. All of the above information is crucial for setting up air quality management strategies and policies. It should be noted that, by only taking into account trajectories within the PBL, the emission retrieval is restricted to a limited range in space. However, improvements can be made by using measurements from several sites and combining the results, which would compensate for the lack in spatial coverage and the accuracy of the retrieval. The horizontal resolution of the retrieval might be improved either by applying higher spatial resolution mesoscale modelling or by replacing the simple backward trajectory model with more complicated trajectory models including dispersion processes.

The uncertainties of the retrieval induced by the in-situ measurements, the modelled PBLH, the wet deposition parameterization and trajectory modelling are discussed. Results show that in-situ measurements of CO and BC bear errors below 0.1ppm and 12%, respectively. According to literature (Hu et al., 2010; García-Díez et al., 2011; Wu et al., 2011), the WRF model underestimates the PBLH under stable conditions. On average, an error of 1% in the modelled PBLH results in 1% variation in the derived emissions. The uncertainty of the wet deposition ranges from 0 to 21% across the domain, while the trajectory displacement errors are mostly within 1.5 times the grid size.

Acknowledgements

We gratefully thank the staff of the Wuqing Meteorological Station for their logistic support. Funds for this research were provided by the National Natural Science Foundation of China Project 40875001 and 40775074, the 973 Program (2011CB403402), and the Basic Research Fund of Chinese Academy of Meteorological Sciences (2008Z011).

References

Ackerman, A. S., Toon, O. B., Stevens, D. E., Heymsfield, A. J., Ramanathan, V., and Welton, E. J.: Reduction of tropical cloudiness by soot, Science, 288, 2000.

Akimoto, H., Ohara, T., Kurokawa, J., and Horii, N.: Verification of energy consumption in China during 1996-2003 by using satellite observational data, Atmos. Environ., 40, 7663-7667, 2006.

Ara Begum, B., Kim, E., Jeong, C.-H., Lee, D.-W., and Hopke, P. K.: Evaluation of the potential source contribution function using the 2002 Quebec forest fire episode, Atmospheric Environment, 39, 3719-3724, 10.1016/j.atmosenv.2005.03.008, 2005.

Ashbaugh, L. L.: A statistical trajectory technique for determining air pollution source regions, J. Air Pollut. Control. Ass., 33, 1096-1098, 1983.

Ashbaugh, L. L., Malm, W. C., and Sadeh, W. Z.: A residence time probability analysis of sulfur concentrations at grand Canyon National Park, Atmospheric Environment (1967), 19, 1263-1270, 10.1016/0004-6981(85)90256-2, 1985.

Baumann, K., and Stohl, A.: Validation of a long-range trajectory model using gas balloon tracks from the Gordon Bennett Cup 95, Jounal of Applied Meteorology and Climatology, 36, 711-720., 1997.

Brioude, J., Kim, S. W., Angevine, W. M., Frost, G. J., Lee, S. H., McKeen, S. A., Trainer, M., Fehsenfeld, F. C., Holloway, J. S., Ryerson, T. B., Williams, E. J., Petron, G., and Fast, J. D.: Top-down estimate of anthropogenic emission inventories and their interannual variability in Houston using a mesoscale inverse modeling technique, J. Geophys. Res., 116, D20305, 10.1029/2011jd016215, 2011.

Constantin, A.: Estimates of sulfate aerosol wet scavenging coefficient for locations in the Eastern United States, Atmospheric Environment, 38, 795-804, 10.1016/j.atmosenv.2003.10.035, 2004.

Cooke, W. F., and Wilson, J. J. N.: A global black carbon aerosol model, J. Geophys. Res., 101, 19395-19409, 10.1029/96jd00671, 1996.

de Foy, B., Lei, W., Zavala, M., Volkamer, R., Samuelsson, J., Mellqvist, J., Galle4, B., Martinez, A.-P., Grutter, M., Retama, A., and Molina, L. T.: Modelling constraints on the emission inventory and on vertical dispersion for CO and SO2 in the Mexico City Metropolitan Area using Solar FTIR and zenith sky UV spectroscopy, Atmos. Chem. Phys., 7, 781–801, 2007.

Draxler, R. R., and Hess, G. D.: Description of the HYSPLIT_4 modeling system, NOAA Tech. Memo, ERL ARL-224, NOAA Air Resources Laboratory, Silver Spring, MD, 24 pp., 1997.

Draxler, R. R., and Hess, G. D.: An overview of the HYSPLIT_4 modelling system for trajectories, dispersion and deposition, Australian Meteorological Magazine, 47, 295-308, 1998.

Draxler, R. R.: HYSPLIT4 user's guide, NOAA Tech. Memo, ERL ARL-230, NOAA Air Resources Laboratory, Silver Spring, MD, 1999.

Dudhia, J.: Numerical study of convection observed during winter monsoon experiment using a mesoscale two-dimensional model, J. Atmos. Sci., 46, 3077-3107, 1989.

Dudhia, J.: A multi-layer soil temperature model for MM5, Preprint from the Sixth PSU/NCAR Mesoscale Model Users' Workshop, 1996.

Eckhardt, S., Prata, A. J., Seibert, P., Stebel, K., and Stohl, A.: Estimation of the vertical profile of sulfur dioxide injection into the atmosphere by a volcanic eruption using satellite column measurements and inverse transport modeling, Atmos. Chem. Phys., 8, 3881-3897, 10.5194/acp-8-3881-2008, 2008.

García-Díez, M., Fernández, J., Fita, L., and Yagüe, C.: WRF skill over Europe with 3 PBL schemes during the year 2001, 3rd International Meeting on Meteorology and Climatology of the Mediterranean, 2011.

Harris, J. M., and Kahl, J. D.: A descriptive atmospheric transport climatology for the Mauna Loa Observatory, using clustered trajectories, J. Geophys. Res., 95, 13651-13667, 1990.

Hitzenberger, R., and Tohno, S.: Comparison of black carbon (BC) aerosols in two urban areas – concentrations and size distributions, Atmospheric Environment, 35, 2153-2167, 10.1016/s1352-2310(00)00480-5, 2001.

Hong, S. Y., Noh, Y., and Dudhia, J.: A new vertical diffusion package with explicit treatment of entrainment processes, Mon. Wea. Rev., 134, 2318-2341, 2006.

Hu, X.-M., Nielsen-Gammon, J. W., and Zhang, F.: Evaluation of Three Planetary Boundary Layer Schemes in the WRF Model, Journal of Applied Meteorology and Climatology, 49, 1831-1844, 10.1175/2010jamc2432.1, 2010.

Jacobson, M. Z.: Strong radiative heating due to the mixing state of black carbon in atmospheric aerosols, Nature, 409, 695-697, 2001.

Kain, J. S., and Fritsch, J. M.: Convective parameterization for mesoscale models: The Kain-Fritcsh scheme, in: The representation of cumulus convection in numerical models, edited by: Emanuel, K. A., and Raymond, D. J., Amer. Meteor. Soc., 246, 1993.

Kuwata, M., and Kondo, Y.: Dependence of size-resolved CCN spectra on the mixing state of nonvolatile cores observed in Tokyo, J. Geophys. Res., 113, D19202, 10.1029/2007jd009761, 2008.

Lee, C., Martin, R. V., van Donkelaar, A., Lee, H., Dickerson, R. R., Hains, J. C., Krotkov, N., Richter, A., Vinnikov, K., and Schwab, J. J.: SO2 emissions and lifetimes: Estimates from inverse modeling using in situ and global, space-based (SCIAMACHY and OMI) observations, J. Geophys. Res., 116, D06304, 10.1029/2010jd014758, 2011.

Lin, W., Xu, X., Ge, B., and Zhang, X.: Characteristics of gaseous pollutants at Gucheng, a rural site southwest of Beijing, J. Geophys. Res., 114, D00G14, 10.1029/2008jd010339, 2009.

Lin, Y., Zhao, C., Peng, L., and Fang, Y.: A new method to calculate monthly CO emissions using MOPITT satellite data, Chinese Sci. Bull., 52, 2551-2558, 2007.

Liu, P. F., Zhao, C. S., Göbel, T., Hallbauer, E., Nowak, A., Ran, L., Xu, W. Y., Deng, Z. Z., Ma, N., Mildenberger, K., Henning, S., Stratmann, F., and Wiedensohler, A.: Hygroscopic properties of aerosol particles at high relative humidity and their diurnal variations in the North China Plain, Atmos. Chem. Phys., 11, 3479-3494, 10.5194/acp-11-3479-2011, 2011.

Lucey, D., Hadjiiski, L., Hopke, P. K., Scudlark, J. R., and Church, T.: Identification of sources of pollutants in precipitation measured at the mid-Atlantic US coast using potential source contribution function (PSCF), Atmospheric Environment, 35, 3979-3986, 10.1016/s1352-2310(01)00185-6, 2001.

Ma, N., Zhao, C. S., Nowak, A., Müller, T., Pfeifer, S., Cheng, Y. F., Deng, Z. Z., Liu, P. F., Xu, W. Y., Ran, L., Yan, P., Göbel, T., Hallbauer, E., Mildenberger, K., Henning, S., Yu, J., Chen, L. L., Zhou, X. J., Stratmann, F., and Wiedensohler, A.: Aerosol optical properties in the North China Plain during HaChi campaign: an in-situ optical closure study, Atmos. Chem. Phys., 11, 5959-5973, 10.5194/acp-11-5959-2011, 2011.

McQueen, J. T., and Draxler, R. R.: Evaluation of model back trajectories of the Kuwait oil fires smoke plume using digital satellite data, Atmos. Environ., 28, 2159-2174, 1994.

Miller, J. M.: A five-year climatology of back trajectories from the Mauna Loa observatory, Hawaii, Atmos. Environ., 15, 1553-1558, 1981.

Mlawer, E. J., Taubman, S. J., Brown, P. D., Iacono, M. J., and Clough, S. A.: Radiative transfer for inhomogeneous atmosphere: RRTM, a validated correlated-k model for the longwave, J. Geophys. Res., 102 16663-16682, 1997.

Moody, J. L., and Samson, P. J.: The influence of atmospheric transport on precipitation chemistry at two sites in the midwestern United States, Atmos. Environ., 23, 2117-2132, 1989.

Petzold, A., and Schönlinner, M.: Multi-angle absorption photometry—a new method for the measurement of aerosol light absorption and atmospheric black carbon, Journal of Aerosol Science, 35, 421-441, 10.1016/j.jaerosci.2003.09.005, 2004.

Petzold, A., Schloesser, H., Sheridan, P. J., Arnott, W. P., Ogren, J. A., and Virkkula, A.: Evaluation of Multiangle Absorption Photometry for Measuring Aerosol Light Absorption, Aerosol Science and Technology, 39, 40-51, 10.1080/027868290901945, 2005.

Ramanathan, V., and Carmichael, G.: Global and regional climate changes due to black carbon, Nature Geosci., 1, 221-227, 2008.

Sander, R.: Compilation of Henry's Law Constants for Inorganic and Organic Species of Potential Importance in Environmental Chemistry (Version 3): http://www.henrys-law.org, 1999.

Seibert, P., Kromp-Kolb, H., Baltensperger, U., Jost, D. T., Schwikowski, M., Kasper, A., and H., P.: Trajectory analyses of aerosol measurements at high alpine sites, in: Transport and Transformation of Pollutants in the Troposphere, edited by: Borrell, P. M., Borrell, P., Cvitas, T., and Seiler, W., Academic Publishing, Den Haag, 689-693, 1994.

Seibert, P.: Inverse modelling of sulfur emissions in Europe based on trajectories, in: Inverse Methods in Global Biogeochemical Cycles, edited by: Kasibhatla, P., Heimann, M., Rayner, P., Mahowald, N., Prinn, R. G., and Hartley, D. E., Geophysical Monograph 114, American Geophysical Union, 147-154, 2000.

Seibert, P.: Inverse modelling with a Lagrangian particle dispersion model: application to point releases over limited time intervals, in: Air Pollution Modeling and its Application XIV, edited by: Schiermeier, F. A., and Gryning, S.-E., Kluwer Academic Publ., 381-389, 2001.

Seibert, P., and Frank, A.: Source-receptor matrix calculation with a Lagrangian particle dispersion model in backward mode, Atmos. Chem. Phys., 4, 51-63, 10.5194/acp-4-51-2004, 2004.

Shiraiwa, M., Kondo, Y., Moteki, N., Takegawa, N., Miyazaki, Y., and Blake, D. R.: Evolution of mixing state of black carbon in polluted air from Tokyo, Geophys. Res. Lett., 34, L16803, 10.1029/2007gl029819, 2007.

Slinn, W. G. N., Hasse, L., Hicks, B. B., Hogan, A. W., Lai, D., Liss, P. S., Munnich, K. O., Sehmel, G. A., and Vittori, O.: Some aspects of the transfer of atmospheric trace constituents past the air-sea interface, Atmos. Environ. , 12, 2055-2087, 1978.

Stohl, A.: Trajectory statistics-A new method to establish source-receptor relationships of air pollutants and its application to the transport of particulate sulfate in Europe, Atmospheric Environment, 30, 579-587, 10.1016/1352-2310(95)00314-2, 1996.

Stohl, A.: Computation, accuracy and applications of trajectories—A review and bibliography, Atmospheric Environment, 32, 947-966, 10.1016/s1352-2310(97)00457-3, 1998.

Stohl, A., and Seibert, P.: Accuracy of trajectories as determined from the conservation of meteorological tracers, Quarterly Journal of the Royal Meteorological Society, 124, 1465-1484, 10.1002/qj.49712454907, 1998.

Stohl, A., Seibert, P., Arduini, J., Eckhardt, S., Fraser, P., Greally, B. R., Lunder, C., Maione, M., Mühle, J., O'Doherty, S., Prinn, R. G., Reimann, S., Saito, T., Schmidbauer, N., Simmonds, P. G., Vollmer, M. K., Weiss, R. F., and Yokouchi, Y.: An analytical inversion method for determining regional and global emissions of greenhouse gases: Sensitivity studies and application to halocarbons, Atmos. Chem. Phys., 9, 1597-1620, 10.5194/acp-9-1597-2009, 2009.

Streets, D. G., Gupta, S., Waldhoff, S. T., Wang, M. Q., Bond, T. C., and Yiyun, B.: Black carbon emissions in China, Atmospheric Environment, 35, 4281-4296, 10.1016/s1352-2310(01)00179-0, 2001.

Tang, G., Li, X., Wang, Y., Xin, J., and Ren, X.: Surface ozone trend details and interpretations in Beijing, 2001–2006, Atmos. Chem. Phys., 9, 8813-8823, 10.5194/acp-9-8813-2009, 2009.

Wang, S. W., Zhang, Q., Streets, D. G., He, K. B., Martin, R. V., Lamsal, L. N., Chen, D., Lei, Y., and Lu, Z.: Growth in NOx emissions from power plants in China: bottom-up estimates and satellite observations, Atmos. Chem. Phys. Discuss., 12, 45-91, 10.5194/acpd-12-45-2012, 2012.

Wu, W., Liu, Y., Vandenberghe, F., Bourgeois, A., Grim, J., Warner, T., Knievel, J., Dudhia, J., Bruyere, C., Stauffer, D., Padovani, M., Luft, G., and Fling, K.: Evaluating PBL Schemes in WRF3.2, WRF workshop, 2011.

Xu, W. Y., Zhao, C. S., Ran, L., Deng, Z. Z., Liu, P. F., Ma, N., Lin, W. L., Xu, X. B., Yan, P., He, X., Yu, J., Liang, W. D., and Chen, L. L.: Characteristics of pollutants and their correlation to meteorological conditions at a suburban site in the North China Plain, Atmos. Chem. Phys., 11, 4353-4369, 10.5194/acp-11-4353-2011, 2011.

Yu, H., Wu, C., Wu, D., and Yu, J. Z.: Size distributions of elemental carbon and its contribution to light extinction in urban and rural locations in the pearl river delta region, China, Atmos. Chem. Phys., 10, 5107-5119, 10.5194/acp-10-5107-2010, 2010.

Zeng, Y., and Hopke, P. K.: A studyof the sources of acid precipitation in Ontario, Canada, Atmos. Environ., 23, 1499-1509, 1989.

Zhang, Q., Streets, D. G., Carmichael, G. R., He, K. B., Huo, H., Kannari, A., Klimont, Z., Park, I. S., Reddy, S., Fu, J. S., Chen, D., Duan, L., Lei, Y., Wang, L. T., and Yao, Z. L.: Asian emissions in 2006 for the NASA INTEX-B mission, Atmos. Chem. Phys., 9, 5131-5153, 10.5194/acp-9-5131-2009, 2009.

Zhao, B., Wang, P., Ma, J. Z., Zhu, S., Pozzer, A., and Li, W.: A high-resolution emission inventory of primary pollutants for the Huabei region, China, Atmos. Chem. Phys., 12, 481-501, 10.5194/acp-12-481-2012, 2012.

Zhou, L., Hopke, P. K., and Liu, W.: Comparison of two trajectory based models for locating particle sources for two rural New York sites, Atmospheric Environment, 38, 1955-1963, 10.1016/j.atmosenv.2003.12.034, 2004.

Table 1. Mean, minimum and maximum values of the average emissions during 13 Jul. -14 Aug 2009 and the according INTEX-B inventory emissions for Beijing, Tianjin Municipality and several sectors of Hebei Province.

Region	*CO (10^{12} μg·hr^{-1})*						*BC (10^{10} μg·hr^{-1})*					
	Mean		*Min.*		*Max.*		*Mean*		*Min.*		*Max.*	
	a	*b*	*a*	*b*	*a*	*b*	*a*	*b*	*a*	*b*	*a*	*b*
Tianjin	21.1	7.1	7.8	2.0	51.6	19.8	7.7	5.8	4.2	1.7	13.5	15.8
Beijing	14.2	8.1	8.3	5.1	22.2	12.2	6.3	6.2	3.8	2.7	7.6	12.0
Hebei-Langfang	21.2	6.9	20.1	4.9	22.9	10.1	8.3	4.8	7.9	3.5	8.9	6.1
Hebei-NE	25.5	5.0	7.6	2.0	41.4	11.4	7.4	4.4	1.7	1.7	12.9	9.9
Hebei-S <100km	13.7	4.9	8.9	2.0	21.6	7.6	6.5	4.2	4.5	1.8	10.9	6.3
Hebei-S >=100km	12.4	5.0	4.2	0.4	30.2	8.8	6.3	4.4	2.9	0.3	16.7	7.3

[a] refers to results from this study

[b] refers to values obtained from the INTEX-B inventory (Zhang et al., 2009)

Table 2. Mean, minimum and maximum standard deviation of the derived emission field for Beijing, Tianjin Municipality and several sectors of Hebei Province.

Region	*Standard Deviations*					
	CO (10^{12} μg·hr^{-1})			*BC (10^{10} μg·hr^{-1})*		
	Mean	*Min.*	*Max.*	*Mean.*	*Min.*	*Max.*
Tianjin	20.0	10.8	89.3	8.5	3.5	26.0
Beijing	6.5	4.3	18.4	2.9	1.6	3.7
Hebei-Langfang	19.0	17.6	19.5	5.1	2.2	5.3
Hebei-NE	18.9	6.2	62.4	5.5	1.5	11.5
Hebei-S <100km	13.8	8.6	23.6	6.1	4.2	10.8
Hebei-S >=100km	10.3	4.1	19.3	4.6	2.3	11.2

Table 3. Mean, minimum and maximum concentration source contributions and according contribution fractions of local emissions and transport from Beijing, Tianjin Municipality and several sectors of Hebei Province.

Location	*CO* *Concentration Contribution[ppb·day^{-1}] (Fraction [%])*						*BC* *Concentration Contribution [μg·m^{-3}·day^{-1}] (Fraction [%])*					
	Mean		*Min.*		*Max.*		*Mean*		*Min.*		*Max.*	
Tianjin	507.0	(54.7)	72.1	(43.9)	4123.8	(77.2)	2.5	(52.3)	0.4	(35.0)	21.0	(76.6)
Beijing	66.4	(7.2)	6.3	(3.8)	206.0	(3.9)	0.3	(7.3)	0.0	(5.9)	0.9	(3.2)
Hebei-Langfang	82.6	(8.9)	39.5	(24.0)	118.9	(2.2)	0.4	(9.0)	0.2	(23.5)	0.6	(2.1)
Hebei-NE	77.2	(8.3)	4.8	(3.0)	197.6	(3.7)	0.3	(6.5)	0.0	(2.4)	0.9	(2.7)
Hebei-S(d<100km)	148.5	(16.0)	38.2	(23.3)	577.5	(10.8)	0.9	(18.8)	0.3	(30.0)	3.2	(12.6)
Hebei-S(d>=100km)	45.9	(4.9)	3.2	(2.0)	121.1	(2.3)	0.3	(6.1)	0.0	(3.2)	0.8	(2.9)
Total	927.6	(100.0)	164.1	(100.0)	5344.9	(100.0)	4.7	(100.0)	1.0	(100.0)	27.4	(100.0)

Figure 1. Time series of hourly average black carbon mass concentration (a), CO volume mixing ratio (b), wind speed and wind direction (c), WRF PBLH (d) and accumulated hourly precipitation (e).

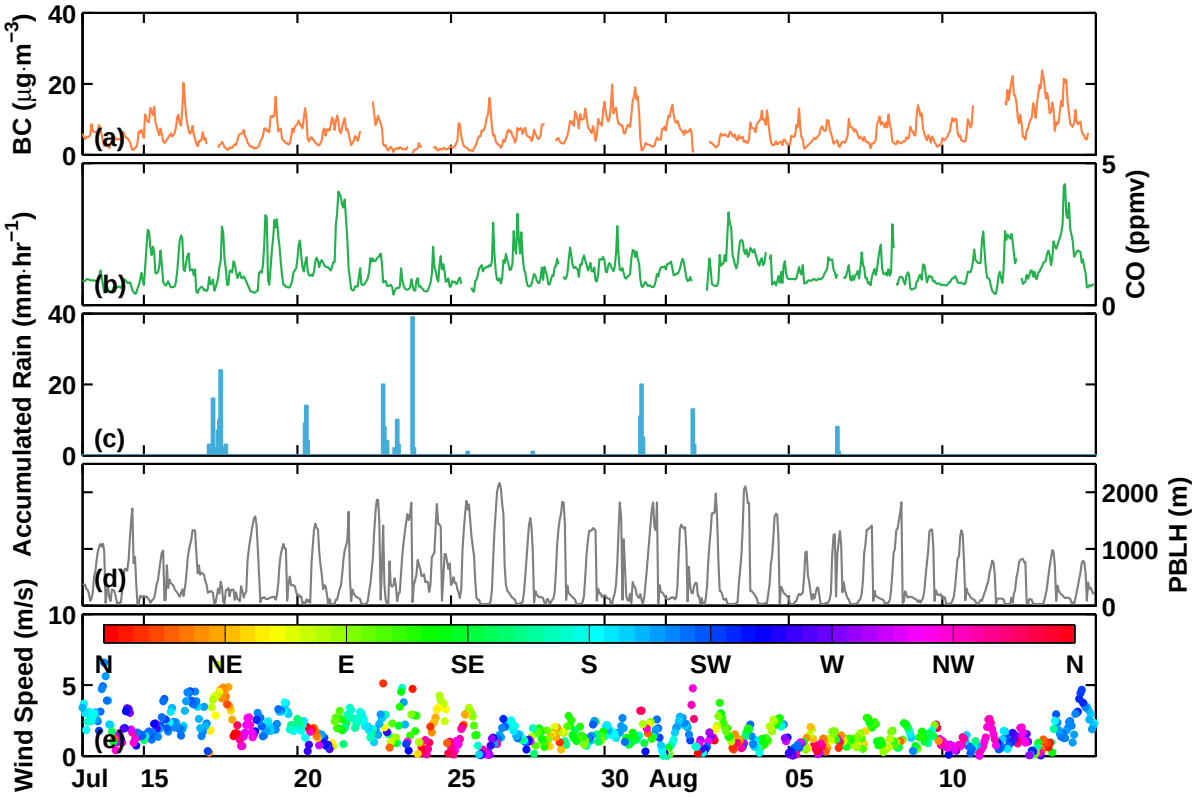

Figure 2. (a) Model domains for the ARW meteorology simulations and the locations of Beijing and Tianjin Municipality and Hebei Province. The green box shows the coarse domain at 18km spatial resolution and the orange box shows the finer domain at 6km spatial resolution. (b) Average MODIS AOD distribution in 2009 (c) Average OMI NO_2 column amount distribution in 2009.

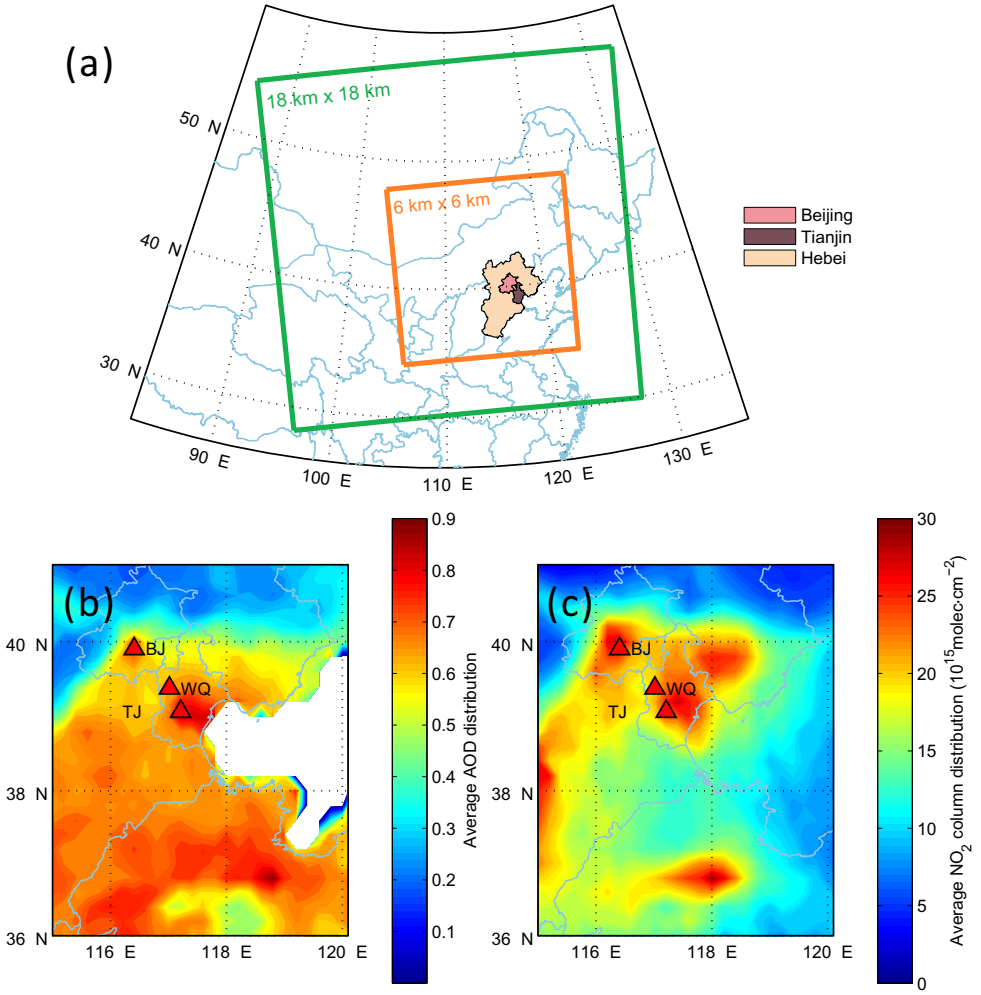

Figure 3. (a) Schematic showing the determination of the PBL residence time of trajectories, where t_1-t_n stand for the time points associated with the n endpoints of trajectory l, C_l is the concentration observed at t_1 (upon arrival of l). The green and purple line shows example trajectories that exceed the boundary layer height during night time and daytime, respectively. (b) Assumption for the diurnal variation of the hydrophilic BC particle fraction.

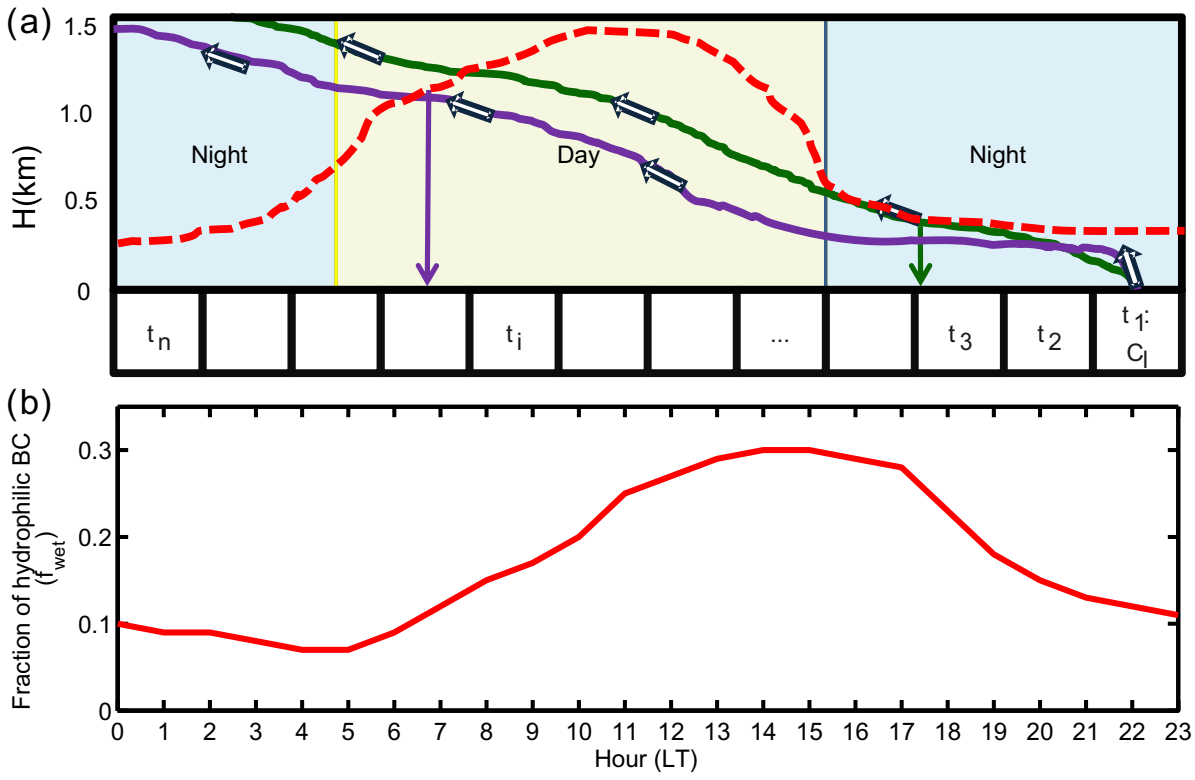

Figure 4. Cluster frequency analyses of trajectories during 13Jul. -14 Aug 2009 in the North China Plain. Upper panels (a1-d1) show the trajectories in each cluster and the mean path of the clusters. Lower panels (a2-d2) show the trajectory heights vs. travel time and the according frequency distribution of all trajectories in each cluster.

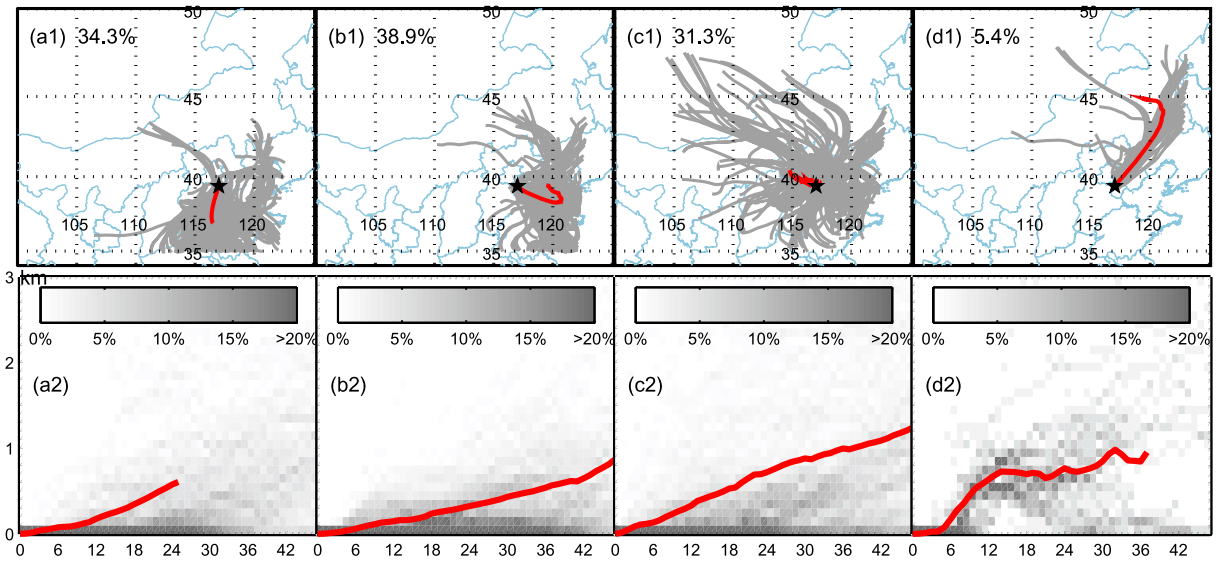

Figure 5. 2006 INTEX-B total emission inventory of BC (a1) and CO (b1) and estimated mean emission field of BC (a2-a4) and CO (b2-b4) during 13 Jul. -14 Aug 2009 in the North China Plain. The second column represents the derived emission fields without using any weighting factor, while the third and fourth column respectively represent the results after using MODIS AOD and OMI NO_2 column as weighting factor.

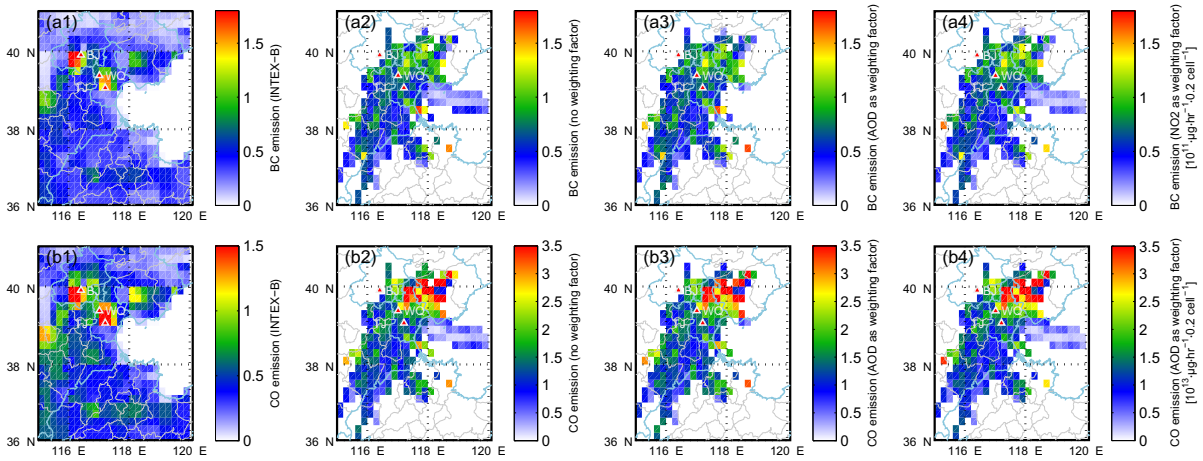

Figure 6. The variation of the emission field induced by the changes in the PBLH field. The circles, boxes and lines represent the median values, the 25th-75th percentile range and the 5th-95th percentile range, respectively.

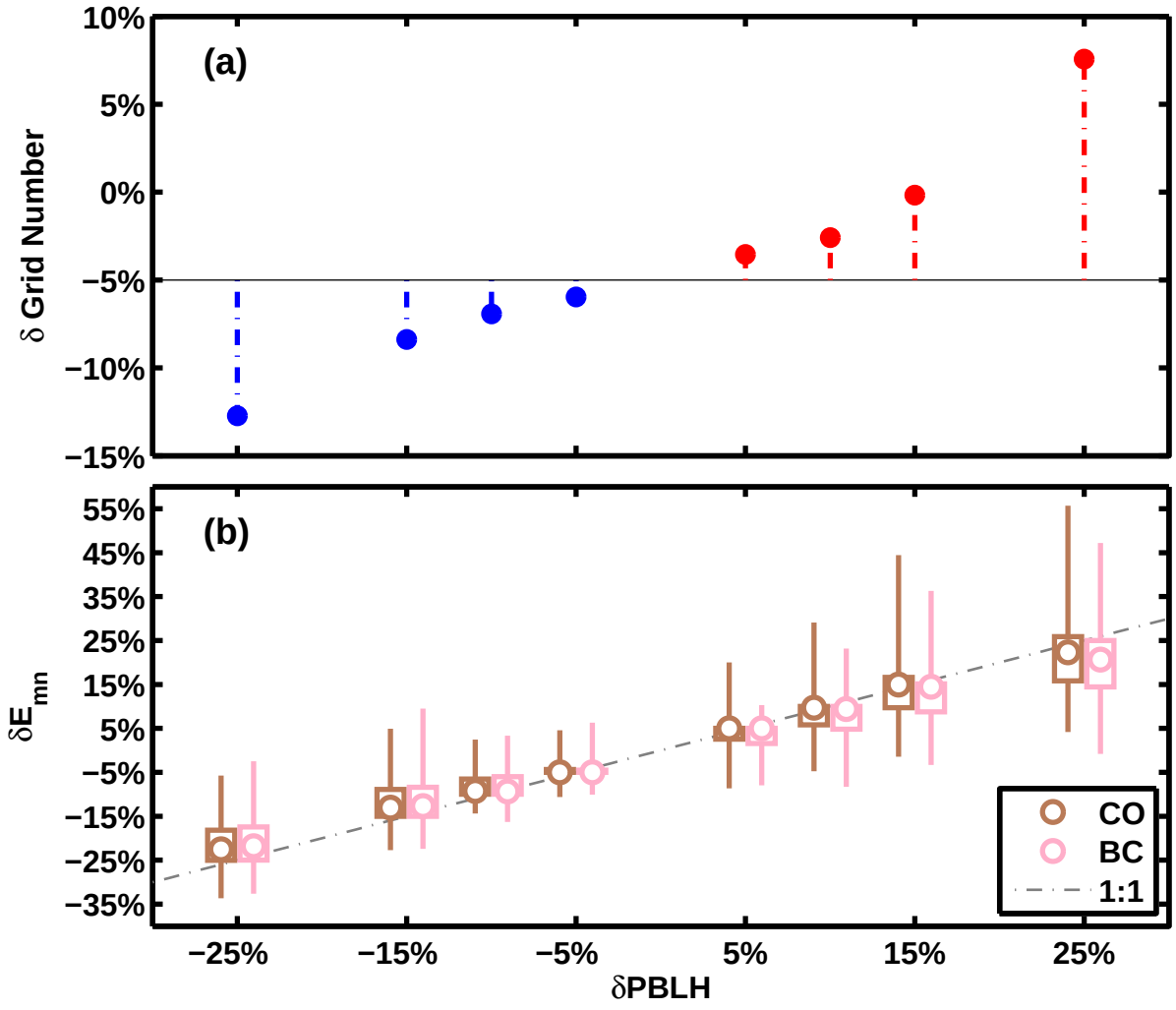

Figure 7. (a) The occurrences of position error (turquoise line) and travel time (pink line) in the derived emissions. (b) Accumulated occurrences of position error (turquoise dotted line) and travel time (pink dotted line) in the derived emissions.